Article

2D Correlation Deep UV Resonance Raman Spectroscopy of Early Events of Lysozyme Fibrillation: Kinetic Mechanism and Potential Interpretation Pitfalls

Victor A. Shashilov, and Igor K. Lednev

J. Am. Chem. Soc., **2008**, 130 (1), 309-317 • DOI: 10.1021/ja076225s

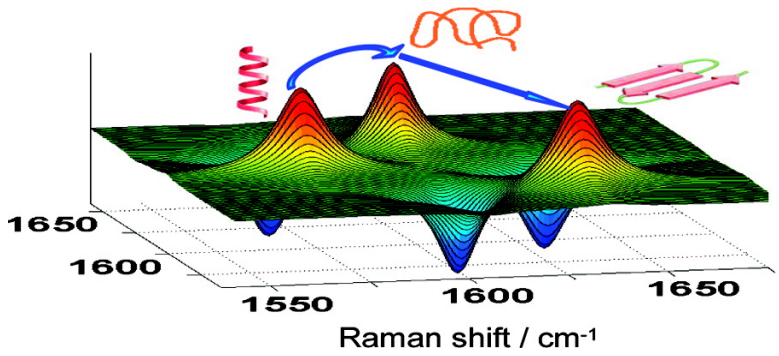

More About This Article

Additional resources and features associated with this article are available within the HTML version:

- Supporting Information
- Links to the 2 articles that cite this article, as of the time of this article download
- Access to high resolution figures
- Links to articles and content related to this article
- Copyright permission to reproduce figures and/or text from this article

View the Full Text HTML

J|A|C|S
ARTICLES
Published on Web 12/08/2007

2D Correlation Deep UV Resonance Raman Spectroscopy of Early Events of Lysozyme Fibrillation: Kinetic Mechanism and Potential Interpretation Pitfalls

Victor A. Shashilov and Igor K. Lednev*

Department of Chemistry, University at Albany, SUNY, 1400 Washington Avenue, Albany, New York 12222

Received August 17, 2007; E-mail: lednev@albany.edu

Abstract: The early stages of hen egg white lysozyme (HEWL) fibrillation were quantitatively characterized by two-dimensional correlation deep UV resonance Raman spectroscopy (2D-DUVRR) in terms of the sequential order of events and their characteristic times. The evolution of individual secondary structural elements was established through the correlation between Amide I, Amide III, and $C_\alpha-H$ bending Raman bands. The temporal order of tertiary and individual secondary structural changes was probed through the cross-correlation of phenylalanine and Amide Raman bands. Both the sequential order and the characteristic times of tertiary and secondary structural changes allowed for reconstructing the molecular mechanism of lysozyme structural changes at the early stages of fibrillation. The 2D-DUVRR analysis of our data indicated that melting of the α-helix happened after the formation of the disordered structure, which was termed as *apparent inverse order* of secondary structural changes. We demonstrated that this apparent inverse order of events is typical for all chemical reactions involving the formation of intermediate(s), which may lead to the serious misinterpretation of 2D correlation results. We proposed a new simulation-aided approach for reconstructing and quantitatively characterizing the reaction mechanism of a (bio)chemical reaction that accounts for the apparent inverse order of events.

Introduction

Studying the early events of fibrillation is crucial for understanding the molecular forces driving the pathogenic process at its nucleation step. It is well-established now that fibrillation is initiated by the partial destabilization of protein structure and proceeds through the nucleus formation followed by the rapid elongation of a fibril.[1] Despite the numerous studies, the detailed molecular mechanism of fibril formation is still far from complete understanding.

Optical biophysical methods such as solution FT-IR[2,3] and CD[2,4,5] have been extensively utilized for studying the molecular mechanism of amyloid fibril formation. However, the light scattering nature of the samples of amyloid fibrils poses serious restrictions for the application of these conventional techniques. In addition, the quantitative analysis of CD spectral data is complicated by the absence of good model spectra of a fibrillar β-sheet[6] and the poorly structured nature of protein CD spectra. The heterogeneity and the transient or insoluble nature of the various species formed over the course of fibrillation seriously limit the applicability of the two most powerful methods of structural biology, namely, solution NMR spectroscopy and X-ray diffraction.[7−9]

Raman spectroscopy is able to characterize all stages of the fibrillation process because, by its nature, Raman effect is a light scattering phenomenon. Utilization of UV irradiation around 200 nm enables selective resonance enhancement of vibrational modes from the amide chromophore, the building block of a polypeptide backbone. High sensitivity of DUVRR spectra to the protein secondary structure is based on the extremely complex nature of the coupling of various amide vibrational modes. Deep UV resonance Raman (DUVRR) spectroscopy has become a valuable tool for structural characterization of proteins and polypeptides.[10−13] We have earlier demonstrated that DUVRR spectroscopy can be used for probing structural evolution of an amyloidogenic protein at all stages of fibril formation.[14]

The quantitative information on the protein structural composition retrieved from DUVRR relies on the quality of basis

(1) Chiti, F.; Dobson, C. M. *Annu. Rev. Biochem.* **2006**, *75*, 333−366.
(2) Khurana, R.; Gillespie, J. R.; Talapatra, A.; Minert, L. J.; Ionescu-Zanetti, C.; Millett, I.; Fink, A. L. *Biochemistry* **2001**, *40*, 3525−3535.
(3) Adams, S.; Higgins, A. M.; Jones, R. A. L. *Langmuir* **2002**, *18*, 4854−4861.
(4) Goda, S.; Takano, K.; Yamagata, Y.; Nagata, R.; Akutsu, H.; Maki, S.; Namba, K.; Yutani, K. *Protein Sci.* **2000**, *9*, 369−375.
(5) McLaughlin, R. W.; De Stigter, J. K.; Sikkink, L. A.; Baden, E. M.; Ramirez-Alvarado, M. *Protein Sci.* **2006**, *15*, 1710−1722.
(6) Wilson, D.; Valluzzi, R.; Kaplan, D. *Biophys. J.* **2000**, *78*, 2690−2701.
(7) Dumoulin, M.; Bader, R. *Protein Pept. Lett.* **2006**, *13*, 211−212.
(8) Hirai, M.; Arai, S.; Iwase, H. *J. Phys. Chem. B* **1999**, *103*, 549−556.
(9) Yonezawa, Y.; Tanaka, S.; Kubota, T.; Wakabayashi, K.; Yutani, K.; Fujiwara, S. *J. Mol. Biol.* **2002**, *323*, 237−251.
(10) Chi, Z.; Asher, S. A. *J. Phys. Chem. B* **1998**, *102*, 9595−9602.
(11) Asher, S. A. Ultraviolet Raman Spectroscopy. In *Handbook of Vibrational Spectroscopy*; John Wiley & Sons, Ltd.: New York, 2001; pp 557−571.
(12) Lednev, I. K.; Ermolenkov, V. V.; He, W.; Xu, M. *Anal. Bioanal. Chem.* **2005**, *381*, 431−437.
(13) JiJi, R. D.; Balakrishnan, G.; Hu, Y.; Spiro, T. G. *Biochemistry* **2006**, *45*, 34−41.
(14) Xu, M.; Ermolenkov, V. V.; He, W.; Uversky, V. N.; Fredriksen, L.; Lednev, I. K. *Biopolymers* **2005**, *79*, 58−61.

spectra representing the average spectroscopic signature of α-helix, β-sheet, and disordered structure.[15] However, the DUVRR spectra of pure secondary structures are not directly observable in the experiment as no protein is composed of a single type of secondary structure. Difference in the basis spectra obtained based on globular protein[16] and homopolypeptide[17] DUVRR data implies that basis spectra are sensitive to the amino acid sequence and, therefore, may be protein-specific. Moreover, the overlap of basis spectra does not always allow for the accurate deconvolution of the experimental DUVRR spectrum into individual structural components, which complicates the quantitative assessment of protein structural evolution.

The 2D correlation spectroscopy (2DCoS)[18] is a powerful alternative to the approach based on fitting using pure secondary structure spectra. 2DCoS allows for decomposing highly overlapping bands in the Raman spectra of proteins into individual components representing various secondary structure elements, amino acids, and side-chain groups and monitoring their evolution. Correlation among spectral regions permits the correct assignment of vibrational bands to structural motifs of proteins and peptides. Furthermore, 2DCoS provides insight into the sequential order of protein conformation changes,[18] thus making it possible to elucidate the nature of structural transitions and the kinetic reaction mechanism.

Application of 2D-IR and 2D-Raman for Protein Folding Problems. The 2DCoS approach for the analysis of protein data is now widely used.[18] 2D-IR has been effectively applied to determine and characterize the elementary steps of the protein folding process,[19−21] to resolve the highly correlated processes of secondary structure evolution,[20] to discriminate between the fully cooperative and stepwise structural transitions,[22] and to relate protein structural changes with hydration[23] and aggregation[24] processes. 2D-IR combined with hydrogen−deuterium exchange (HX) has been proven to be a valuable tool for characterizing the solvation and structural stability of proteins,[25] resolving complex bands into individual structure-related components,[26] studying protein−lipid interactions,[27] etc. Application of chemometric[28] and novel spectral preprocessing methods[19] for 2D-IR analysis of protein data has also been demonstrated. Advent of femtosecond lasers has paved the way for establishing a new powerful structural technique called multidimensional correlation spectroscopy.[29] Recently, 2D-IR spectroscopy has allowed for probing fibrillar structure[30] and interaction between various structural motifs of fibrils,[31] which can ultimately provide valuable structural information for resolving the atomic resolution structure of amyloid aggregates.

Similarly to IR, Raman spectra exhibit pronounced changes in response to protein secondary and tertiary structural rearrangements. The 2D correlation analysis of Raman data has been utilized to extract the temporal order of folding/unfolding events of the protein structural transition.[32,33] The application of 2D-Raman for fast discriminating of microorganisms has been reported.[34] Well-structured Raman spectra allow for the facile interpretation of spectra from other techniques via relating them by means of the heterospectral 2DCoS approach.[35,36] Thereby, β-turn bands in FT-NIR and FT-Raman spectra were identified,[35] and weak disordered structure and α-helical components of the Amide III band of Raman and IR spectra, respectively, were confidently assigned.[37] Blanch and co-workers have established the approach of correlating Raman optical activity (ROA) and Raman spectra and demonstrated its application for a number of protein folding problems.[33,38,39]

In this work, 2DCoS exhibiting unique spectral resolution enabled us to probe individual secondary structural components at the early stage of lysozyme fibrillation. The effective characteristic times of the evolution of α-helix, disordered structure, and nucleus β-sheet were evaluated. In addition, the relative rate of changes in tertiary and various secondary structures was determined. The kinetic mechanism of structural changes at the early stage of lysozyme fibrillation was reconstructed based on the apparent inverse order of secondary structural changes revealed by 2DCoS and the characteristic times of corresponding intensity changes. The methodology aspect of this study involves the development of the new simulation-aided approach combining the $k\nu$ correlation analysis[40] and modeling the concentration profiles of reactants constrained to the most probable kinetics scheme of the biochemical reaction. Possible applications of this general 2DCoS method for various types of chemical processes and spectroscopic techniques are discussed.

Materials and Methods

Sample Preparation. Hen egg white lysozyme (HEWL) and sodium trifluoroacetate were purchased from Sigma (St. Louis, MO) and used as received. The preparation of lysozyme fibrils was described elsewhere.[14] Briefly, ∼14 mg/mL of lysozyme solution at pH 2.0 was

(15) Chi, Z.; Chen, X. G.; Holtz, J. S. W.; Asher, S. A. *Biochemistry* **1998**, *37*, 2854−2864.
(16) Huang, C.-Y.; Balakrishnan, G.; Spiro, T. G. *J. Raman Spectrosc.* **2006**, *37*, 277−282.
(17) Mikhonin, A. V.; Myshakina, N. S.; Bykov, S. V.; Asher, S. A. *J. Am. Chem. Soc.* **2005**, *127*, 7712−7720.
(18) Noda, I.; Ozaki, Y. *Two-Dimensional Correlation Spectroscopy: Applications in Vibrational and Optical Spectroscopy*; John Wiley & Sons: New York, 2004; p 295.
(19) Zhang, J.; Yan, Y.-B. *Anal. Biochem.* **2005**, *340*, 89−98.
(20) Peng, X.; Shao, Z.; Chen, X.; Knight, D. P.; Wu, P.; Vollrath, F. *Biomacromolecules* **2005**, *6*, 302−308.
(21) Ausili, A.; Dilauro, B.; Cobucci-Ponzano, B.; Bertoli, E.; Sciré, A.; Rossi, M.; Tanfani, F.; Moracci, M. *Biochem. J.* **2004**, *384*, 69−78.
(22) Fabian, H.; Mantsch, H. H.; Schultz, C. P. *Proc. Natl. Acad. Sci. U.S.A.* **1999**, *96*, 13153−13158.
(23) Murayama, K.; Ozaki, Y. *Biopolymers (Biospectroscopy)* **2002**, *67*, 394−405.
(24) Schultz, C. P.; Barzu, O.; Mantsch, H. H. *Appl. Spectrosc.* **2000**, *54*, 931−938.
(25) DeFlores, L. P.; Tokmakoff, A. *J. Am. Chem. Soc.* **2006**, *128*, 16520−16521.
(26) Gradolnik, J.; Maréchal, Y. *Appl. Spectrosc.* **2005**, *59*, 1347−1356.
(27) Elmore, D. L.; Dluhy, R. A. *J. Phys. Chem. B* **2001**, *105*, 11377−11386.
(28) Domínguez-Vidal, A.; Saenz-Navajas, M. P.; Ayora-Cañada, M. J.; Lendl, B. *Anal. Chem.* **2006**, *78*, 3257−3264.
(29) Mukamel, S. *Annu. Rev. Phys. Chem.* **2000**, *51*, 691−729.
(30) Shim, S.-H.; Strasfeld, D. B.; Ling, Y. L.; Zanni, M. T. *Proc. Natl. Acad. Sci. U.S.A.* **2007**, *104*, 14197−14202.
(31) Zhuang, W.; Abramavicius, D.; Voronine, D. V.; Mukamel, S. *Proc. Natl. Acad. Sci. U.S.A.* **2007**, *104*, 14233−14236.
(32) Zhou, P.; Xie, X.; Knight, D. P.; Zong, X.-H.; Deng, F.; Yao, W.-H. *Biochemistry* **2004**, *43*, 11302−11311.
(33) Ashton, L.; Barron, L. D.; Hecht, L.; Hyde, J.; Blanch, E. W. *Analyst* **2007**, *132*, 468−479.
(34) Mello, C.; Ciuffi, K. J.; Nassar, E.; Ribeiroa, D.; Poppi, R. J. *J. Braz. Chem. Soc.* **2006**, *17*, 73−78.
(35) McClure, W. F.; Maeda, H.; Dong, J.; Liu, Y.; Ozaki, Y. *Appl. Spectrosc.* **1996**, *50*, 467−475.
(36) Kubelka, J.; Pancoska, P.; Keiderling, T. A. *Appl. Spectrosc.* **1999**, *53*, 666−671.
(37) Jung, Y. M.; Shin, H. S.; Kim, S. B.; Noda, I. *Appl. Spectrosc.* **2002**, *56*, 1562−1567.
(38) Ashton, L.; Czarnik-Matusewicz, B.; Blanch, E. W. *J. Mol. Struct.* **2006**, *799*, 61−71.
(39) Ashton, L.; Barron, L. D.; Czarnik-Matusewicz, B.; Hecht, L.; Hyde, J.; Blanch, E. W. *Mol. Phys.* **2006**, *104*, 1429−1445.
(40) Shanmukh, S.; Dluhy, R. A. *J. Phys. Chem. A* **2004**, *108*, 5625−5634.

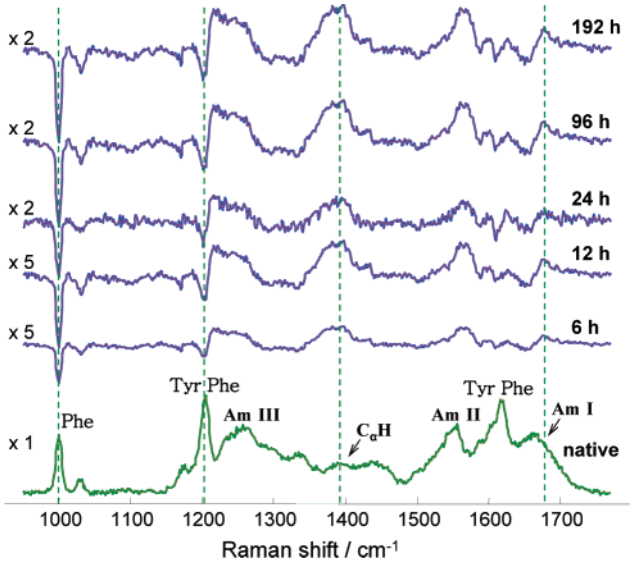

Figure 1. Native (bottom) and difference spectra of HEWL recorded at various incubation times. Amide I band (AM I) consists of carbonyl C═O stretching, with a small contribution from C−N stretching and N−H bending; Amide II (AM II) and Amide III (AM III) bands involve significant C−N stretching, N−H bending, and C−C stretching; The C_α−H bending vibrational mode involves C_α−H symmetric bending and C−C_α stretching.[11] Phe: phenylalanine; Tyr: tyrosine.

prepared and incubated at 65 °C for various durations.[14,41] The incubated solutions were centrifuged at 16 000*g* for 30 min to separate the soluble fraction from the gelatinous fraction that is dominated by fibrils. The soluble fraction was directly used for Raman spectroscopic measurements as the partially unfolded intermediate and the fibrillation nucleus have been shown to remain in a thermodynamic equilibrium in solution.[42]

DUVRR Measurements. A home-built DUVRR spectroscopic apparatus was described in details elsewhere.[12] The 197 nm fourth harmonic generation of Indigo S laser system (Coherent, Inc.) was used for excitation. Raman scattering was dispersed and recorded using a home-built double monochromator coupled with a liquid-nitrogen-cooled CCD camera (Roper Scientific, Inc.). A rotating Suprasil NMR tube with a magnetic stirrer inside was used as a sample holder. The acquired Raman spectra were analyzed using GRAMS/AI software (Thermo Electron Corp.). Spectral contributions of water and quartz were numerically subtracted. Sodium trifluoroacetate was used as the internal standard for intensity normalization.

2D-DUVRR Analysis. GRAMS/AI software (Thermo Galactic) was used for the numerical subtraction of the spectral contribution of water and quartz. 2DCoS studies were performed using homemade programs operating in the Matlab environment. Four sets of lysozyme DUVRR spectra recorded at different time increments and in different incubation time ranges were used to construct data matrices for 2DCoS analysis, with each dataset consisting of at least 21 DUVRR spectra.

Results and Discussion

DUVRR Spectra of HEWL at the Early Stage of Fibrillation. The DUVRR spectrum of native lysozyme and selected differential DUVRR spectra of lysozyme recorded over the course of incubation are shown in Figure 1. The HEWL DUVRR spectroscopic signature is composed of amide vibrational modes (Amide I, Amide II, Amide III, and C_α−H bending) and bands arising from aromatic amino acid side chains. The amide vibrational modes provide information on the protein secondary structure, while phenylalanine, a natural DUVRR spectroscopic biomarker,[14] reports on the tertiary structural evolution. The major structural components of protein DUVRR bands are summarized in Table 1. The Amide I band is of the highest frequency and located at ∼1660 cm^{-1}; Amide II is centered at 1555 cm^{-1}, and the broad Amide III band spans the range of 1220−1320 cm^{-1}. The less intense C_α−H bending band is evident in the region of 1380−1400 cm^{-1}. It is enhanced in DUVRR spectra of the β-sheet and disordered structure and absent in DUVRR spectra of the α-helix. The vibrations of the tyrosine and phenylalanine aromatic residues give rise to sharp intense Raman bands at 1620 and 1205 cm^{-1}. The narrow peak at 1000 cm^{-1} is due to the breathing vibration of the aromatic rings of phenylalanine residues.

Table 1. Major Structural Components of Lysozyme DUVRR Bands

DUVVRR band	spectral position (cm^{-1})	structure[a]
Amide I	1645−1655	α-helix[32,51]
	1660−1670	disordered structure[32,52]
	1673−1675	cross β-sheet[43,44]
C_α−H	1380−1390	disordered structure[42,52]
	1395−1405	cross β-sheet[42,52]
Amide III	1220−1230	cross β-sheet[44,53]
	1240−1260	disordered structure[52,53]
	1290−1310	α-helix[51]
phenylalanine	1000	tertiary structure[14]

[a] The superscripts denote the ref number in the main text.

Major spectral changes throughout the incubation occur in Amide I, C_α−H bending, and 1000 cm^{-1} phenylalanine bands (marked with dotted lines in Figure 1). The Amide I band is gradually up-shifted with incubation time and becomes sharper as clearly seen from the DUVRR spectra corresponding to 96 and 144 h of incubation. Our studies have shown that the Amide I band of native lysozyme[43] is centered at 1660 cm^{-1}, whereas the Amide I bands of unordered lysozyme and lysozyme fibrillar β-sheet have maxima around 1667 and 1674 cm^{-1}, respectively.[44] Accordingly, the high-frequency shift of the Amide I band indicates the increase in disordered structure and/or β-sheet contents over the course of incubation. The noticeable sharpening of the Amide I band at long incubation times is due to the formation of nucleus β-sheet structure[42] (see below).

According to X-ray crystallographic data,[45] native lysozyme contains 62% disordered structure, 32% α-helix, and 6% β-sheet. Disordered structure and β-sheet conformations give rise to a weak C_α−H bending band in the DUVRR spectrum of native protein (Figure 1), while the α-helix makes no contribution in this spectral region.[11] Continuous increase in the intensity of the C_α−H bending band in the DUVRR spectra with incubation time indicates the development of disordered structure and/or β-sheet from α-helix, which is consistent with changes in the Amide I band, too.

Further visual inspection of the DUVRR spectra of lysozyme (Figure 1) reveals a pronounced drop in 1000 cm^{-1} phenyla-

(41) Krebs, M. R. H.; Wilkins, D. K.; Chung, E. W.; Pitkeathly, M. C.; Chamberlain, A. K.; Zurdo, J.; Robinson, C. V.; Dobson, C. M. *J. Mol. Biol.* **2000**, *300*, 541−549.
(42) Shashilov, V.; Xu, M.; Ermolenkov, V. V.; Fredriksen, L.; Lednev, I. K. *J. Am. Chem. Soc.* **2007**, *129*, 6972−6973.
(43) Shashilov, V. A.; Xu, M.; Ermolenkov, V. V.; Lednev, I. K. *J. Quant. Spectrosc. Radiat. Transfer* **2006**, *102*, 46−61.
(44) Xu, M.; Shashilov, V.; Lednev, I. K. *J. Am. Chem. Soc.* **2007**, *129*, 11002−11003.
(45) Artymiuk, P. J.; Blake, C. C. F.; Rice, D. W.; Wilson, K. S. *Acta Crystallogr.* **1982**, *B38*, 778−783.

lanine band intensity, which is indicative of melting of tertiary structure.[14] The 2D correlation analysis was further employed to correlate both the rate of tertiary structure melting with that of secondary structural rearrangements and the relative rates of secondary structural changes.

Previous DUVRR Studies of Lysozyme Fibrillation and Novelty of the Current Study. Previously, we have quantitatively characterized both the partial irreversible unfolding and the nucleation step of fibrillation of hen egg white lysozyme (HEWL), the most studied model of pathogenic protein. In particular, we proved a two-state transition mechanism of lysozyme irreversible unfolding using intrinsic tryptophan fluorescence, DUVRR spectroscopy, and ESI-MS, along with comprehensive chemometric analysis of the experimental data.[46] Furthermore, we monitored the formation of nucleus β-sheet by using DUVRR spectroscopy combined with 2DCoS analysis of the $C_\alpha-H$ bending band and advanced spectral separation methods.[42] The latter study has proven that the early events of lysozyme fibrillation follow the scheme proposed by Dobson and co-workers[47] and enabled the determination of species-specific kinetic profiles in the early stages of fibril formation and extraction of the rate constants for each process.[42] That approach allowed us to quantitatively describe the early events of lysozyme fibrillation in terms of the evolution of native lysozyme, the partially unfolded intermediate, and the β-sheet-rich nucleus. Each of these individual species, nevertheless, is still a combination of presumably three major secondary structures, that is, an α-helix, a disordered structure, and a β-sheet. In fact, spectral separation methods cannot decompose DUVRR spectra into those of pure secondary structures because of the rotational ambiguity property. The latter means that extracting the set of true basis spectra is extremely difficult as there are numerous different three-spectrum sets that can fit experimental data equally well. Therefore, the determined rate constants[42] reported the average rate of secondary and tertiary structural changes in each of the individual species.

Here we quantitatively describe the early stage of lysozyme fibrillation in terms of evolution of elementary secondary structures, α-helix, disordered structure, and β-sheet, and the tertiary structure of lysozyme, which is a next step toward the detailed understanding of the process on the molecular level. In fact, the 2DCoS approach allows for decomposing highly overlapping Amide I, Amide III, and $C_\alpha-H$ bending Raman bands into individual secondary structural elements[18,33] and monitoring them independently. This was made possible because of the high sensitivity of the 2D correlation maps to subtle spectral changes such as band broadening, band shift, or asynchronous intensity changes in different spectral regions.[48] All of these effects are often overlooked by conventional spectral resolution methods, while they can be crucial for understanding the nature of biochemical processes under study.

Two-Dimensional Correlation Analysis of Lysozyme DUVRR Spectral Data. Although the 2DCoS analysis was performed independently on four DUVRR datasets and yielded consistent qualitative and quantitative findings, 2D correlation maps and discussion below refer to a single dataset having the highest signal-to-noise ratio.

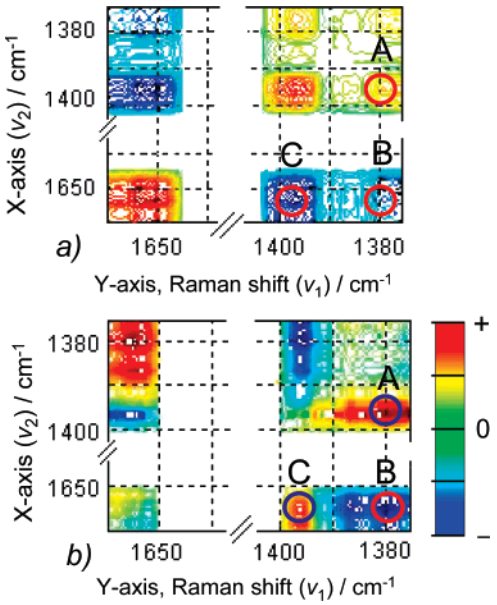

Figure 2. Synchronous (a) and asynchronous (b) 2D-DUVRR maps of the $C_\alpha-H$ bending band and α-helix sub-band of the Amide I region.

Amide I/$C_\alpha-H$ Cross-Correlation. As seen from Table 1, only the disordered structure and β-sheet contribute to the $C_\alpha-H$ bending DUVRR region, which simplifies the 2DCoS analysis of this region. Figure 2 shows the results of correlation between the $C_\alpha-H$ bending and the α-helix region of Amide I.

To reduce the complexity of 2D correlation maps, they were constructed by concatenating the regions under study, leaving out non-informative ones. The double slash (//) marks the axis breaks on 2D correlation plots. Positive and negative regions on the 2D maps are shown with red and blue, respectively, according to the color bar in Figure 2. Three autopeaks are clearly resolved on the synchronous 2D map (Figure 2a): 1655 cm^{-1} (α-helix), 1380 cm^{-1} (disordered structure), and 1395 cm^{-1} (β-sheet). Hereinafter, we will consider only those cross-peaks that are located below the correlation map diagonal and mark them as ν_y/ν_x, where ν_y and ν_x refer to the *y*- and *x*-axis wavenumber, respectively. The positive sign of the cross-peak at 1380/1395 cm^{-1} (**A**) and the negative sign of 1380/1655 (**B**) and 1395/1655 cm^{-1} (**C**) peaks indicate that intensity changes in the disordered structure and β-sheet regions were positively correlated while the contribution of the α-helix changed in the opposite direction as compared to either disordered structure or β-sheet. This finding is consistent with the melting of the α-helix and the formation of disordered structure and β-sheet structures. The asynchronous 2D map (Figure 2b) was presented following the approach proposed by Blanch and co-workers;[49] namely, the *x*- and *y*-axes were reversed and the *y*-axis was set as a horizontal one. The positive cross-peak at 1380/1395 cm^{-1} (**A**) suggests that spectral changes in the disordered structure region happen first. Taking into account both the negative synchronous peak at 1380/1655 cm^{-1} (**B**) and the negative sign of the 1380/1655 cm^{-1} (**B**) asynchronous peak, one may conclude that changes at 1380 cm^{-1} (disordered structure) occur before those at 1655 cm^{-1} (α-helix). It further turns out that

(46) Xu, M.; Shashilov, V. A.; Ermolenkov, V. V.; Fredriksen, L.; Zagorevski, D.; Lednev, I. K. *Protein Sci.* **2007**, *16*, 815−832.
(47) Booth, D. R.; Sunde, M.; Bellotti, V.; Robinson, C. V.; Hutchinson, W. L.; Fraser, P. E.; Hawkins, P. N.; Dobson, C. M.; Radford, S. E.; Blake, C. C. F.; Pepys, M. B. *Nature* **1997**, *385*, 787−793.
(48) Noda, I. *Vib. Spectrosc.* **2004**, *36*, 143−165.
(49) Czarnik-Matusewicz, B.; Pilorz, S.; Ashton, L.; Blanch, E. W. *J. Mol. Struct.* **2006**, *799*, 253−258.

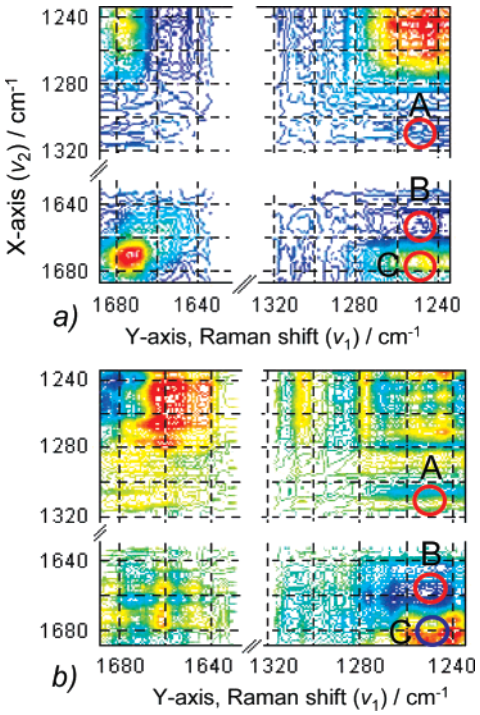

Figure 3. Synchronous (a) and asynchronous (b) 2D-DUVRR maps of the Amide III and Amide I regions.

β-sheet (1395 cm^{-1}) changes after α-helix, as evident from the negative 1395/1655 cm^{-1} (**C**) synchronous spot and the positive 1395/1655 cm^{-1} (**C**) asynchronous cross-peak. Putting the individual sequential orders together, one would come up with the following order of spectral intensity change: disordered structure → α-helix → β-sheet.

Amide I/Amide III Cross-Correlation. The results of spectral intensity correlation of Amide III and Amide I spectral regions are presented in Figure 3a,b. The Amide III region of ~1250 cm^{-1} is normally assigned to disordered structure, 1225 cm^{-1} to antiparallel β-sheet, while the high-frequency tail of Amide III at 1290−1310 cm^{-1} is mainly affected by the α-helix (see Table 1). The negative correlation at 1250/1310 cm^{-1} (**A**) and 1250/1655 cm^{-1} (**B**) supports (Figure 3a) this assignment, demonstrating a decrease in the α-helical fraction and the development of disordered structure over the course of lysozyme incubation. Similarly to Figure 2b, the asynchronous map (Figure 3b) indicates that changes at 1250 cm^{-1} (disordered structure) occur before those of the α-helix at 1655 cm^{-1}. The intense positive speckle at 1250/1675 cm^{-1} (**C**) suggests random changes before the β-sheet that exhibits a sharp peak around 1675 cm^{-1}. The extracted sequential order of secondary structural changes turns out to be the same as that in the case of Amide I/C$_\alpha$−H bending cross-correlation (Figure 2a,b): disordered structure → α-helix → β-sheet.

Aromatic/Amide III Cross-Correlation. Finally, we compared the relative rate of secondary and tertiary structural changes using the Amide III region and the 1000 cm^{-1} phenylalanine band, a probe of lysozyme tertiary structure. Panels a and b of Figure 4 depict the synchronous and asynchronous 2D maps, respectively. The highest correlation on the synchronous map (Figure 4a) is observed at 1000/1000 cm^{-1} (**A**), 1250/1250 cm^{-1} (**B**) autopeaks, and the 1000/1250 cm^{-1} (**C**) cross-peak. The negative sign of the latter shows the opposite directions of intensity changes of the phenylalanine

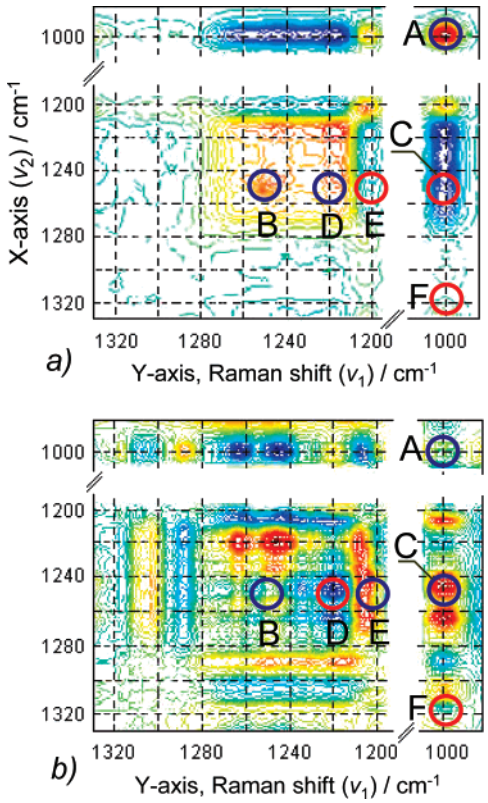

Figure 4. Synchronous (a) and asynchronous (b) 2D-DUVRR maps of the Amide III and phenylalanine (1000 cm^{-1}) regions.

(1000 cm^{-1}) and disordered structure sub-band of Amide III (1250 cm^{-1}). The positive asynchronous region at 1000/1250 cm^{-1} (**C**) (Figure 4b) and the corresponding negative sign on the synchronous map suggest that the phenylalanine band changes after that of disordered structure. Another strong asynchronous peak at 1220/1250 cm^{-1} (**D**) shows that changes at 1220 cm^{-1} are delayed with respect to those at 1250 cm^{-1}. As shown elsewhere,[44] the Amide III band of the fibrillar β-sheet is centered at ~1224 cm^{-1}. Accordingly, the observed temporal order 1250 → 1220 cm^{-1} is consistent with the delay between the appearance of disordered structure and β-sheet observed in this study (Amide I/C$_\alpha$−H correlation, Figure 2b) and reported elsewhere.[42] The aromatic region at 1200 cm^{-1} is a superposition of phenylalanine and tyrosine DUVVRR aromatic bands. Similarly to the 1000 cm^{-1} band, intensity at 1200 cm^{-1} changes after that of disordered structure, resulting in the positive 1200/1250 cm^{-1} (**E**) spot. As opposed to disordered structure versus aromatic band correlation, there are no pronounced asynchronous peaks at 1000/1320 cm^{-1} (**F**). Alternating positive and negative weak speckles in this region arise from noise and a small contribution from a high-frequency tail of the disordered structure of the Amide III band. It is well-known that significant band overlap and noise may complicate the interpretation of correlation diagrams. While the noise level can be significantly reduced by using various smoothing methods, the band overlap problem persists and becomes the major source of misinterpretation of asynchronous 2D correlation maps. The weak double peak in the region of 1280−1320 cm^{-1} in Figure 4b results from overlap of multiple bands in the Amide III$_{(2)}$ helical region and therefore is not significant. This means that α-helix and lysozyme tertiary structure melt at the same rate, while changes

in the unordered parts of the protein occur before changes in the tertiary structure.

Consequently, the 2D correlation analysis performed on Amide I, Amide III, $C_\alpha-H$ bending regions, and the phenylalanine 1000 cm^{-1} band revealed the following sequential order of lysozyme structural changes: disordered structure → α-helix and tertiary structure → β-sheet.

Extraction of Characteristic Times for Evolution of Tertiary and Secondary Structures. The effective rate constants of secondary and tertiary structural changes were retrieved directly from 2D-DUVRR data by means of the $k\nu$ correlation analysis.[40] Briefly, in this approach, the time-dependent concentration profiles are modeled using a basis set of exponential or sinusoidal[27] reference functions. The $k\nu$ correlation analysis allows the quantitative characterization of spectral intensity changes using the concepts of the effective rate constant k_{eff} and has demonstrated excellent performance in detecting small differences in the rates of dynamic intensity changes. The asynchronous correlation of experimental intensities against a reference set of exponentially decaying intensities was performed following the approach described by Shanmukh et al:[40]

$$\Psi(\tau,\nu) = \frac{1}{N-1}\sum_{j=0}^{N-1} y(\nu,n_j)\sum_{k=0}^{N-1} N_{jk} \times \exp(-t/\tau + R)$$

where $\Psi(\tau,\nu)$ is the correlation intensity at some point (τ,ν); N is the total number of spectra; n_j is the order number of the spectrum; τ is the characteristic time of the exponential decay; N_{jk} is the Hilbert−Noda transformation matrix; R is the constant matrix, and $y(\nu,n_j)$ are spectral intensities.

If the characteristic time of the exponential decay at some wavenumber in DUVRR data equals that of the reference intensity, the corresponding asynchronous intensity $\Psi(k,\tau)$ will be zero. Figure 5a shows the $\Psi(\tau,\nu)$ calculated for the $C_\alpha-H$ bending region. For visualization purpose, the natural logarithms of the absolute values of the $\Psi(\tau,\nu)$ were used as the third-dimension coordinate. With this representation, minima on the asynchronous map (blue spots) appear if the effective characteristic time of intensity change at a given wavenumber ν is equal to τ. As seen from Figure 5a, the characteristic time in the $C_\alpha-H$ bending region gradually increases from 21−22 h at 1385 cm^{-1} (disordered structure) to 34−36 h at 1400 cm^{-1} (β-sheet). Applying the $k\nu$ approach to ~1640−1655 and 1000 cm^{-1} spectral regions, we found the characteristic times of the α-helix and tertiary structure melting to be around ~30 h. This means that melting of α-helical and tertiary structures occurred synchronously with $\tau \sim 30$ h, which supports the results of Aromatic/Amide III correlation analysis. The formation of the nucleus β-sheet was delayed to yield a longer effective characteristic time $\tau \sim 34-36$ h, thus being in a good agreement with the qualitative results of 2D analysis described above. To summarize, the lysozyme structural changes were found to proceed via the following sequence of events: disordered structure formation ($\tau \sim 22$ h) → tertiary structure and α-helix melting ($\tau \sim 30$ h) → nucleus β-sheet formation ($\tau \sim 35$ h).

Elucidating the Mechanism of Lysozyme Structural Transition. The 2D correlation analysis described above yielded the temporal order and characteristic times of secondary and tertiary structural evolution of lysozyme at its early stages of fibrillation. In the next step, all of these findings should be used to deduce the kinetic model of lysozyme nucleation, which is the ultimate goal of this study. To accomplish this, the simulation-aided approach for model testing was utilized. In this approach, different kinetic schemes with varying reaction-specific rate constants were used to simulate spectral data and calculate 2D and $k\nu$ correlation maps. The mechanism of lysozyme structural changes was then deduced based on the best match of 2D and $k\nu$ correlation maps for experimental and model-specific simulated data.

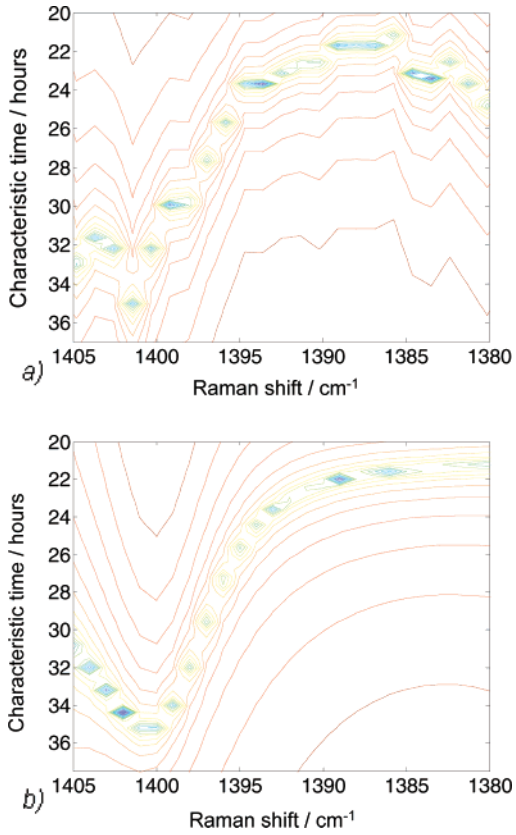

Figure 5. DUVRR (a) and simulated (b) asynchronous $k\nu$ correlation map $\Psi(\tau,\nu)$ of the $C_\alpha-H$ bending region. The blue spots at the intersection of the Raman shift and characteristic time coordinates relate the spectral position with the corresponding characteristic time of spectral intensity change.

At first glance, the obtained temporal order of events involving disordered structure formation ($\tau \sim 22$ h) → tertiary structure and α-helix melting ($\tau \sim 30$ h) → nucleus β-sheet formation ($\tau \sim 35$ h) (hereinafter referred to as *apparent inverse order*) seems meaningless. Obviously, the event of α-helix melting is required to produce any amount of disordered structure, and therefore, the α-helical structure should first respond to temperature destabilization. The explanation to this apparent paradox is straightforward. The asynchronous 2DCoS probes not only the sequential order of events in a chemical reaction but also the average rate of concentration change of each species. This issue is often overlooked when analyzing 2DCoS results, which may lead to the serious misinterpretation of spectroscopic data. In our case, the newly formed disordered structure is a reacting intermediate involved in further transformation to a β-sheet. It is due to β-sheet formation that the effective rate of disordered structure evolution is faster than the rate of α-helix melting. The origin of this apparent inverse order effect is described in detail below.

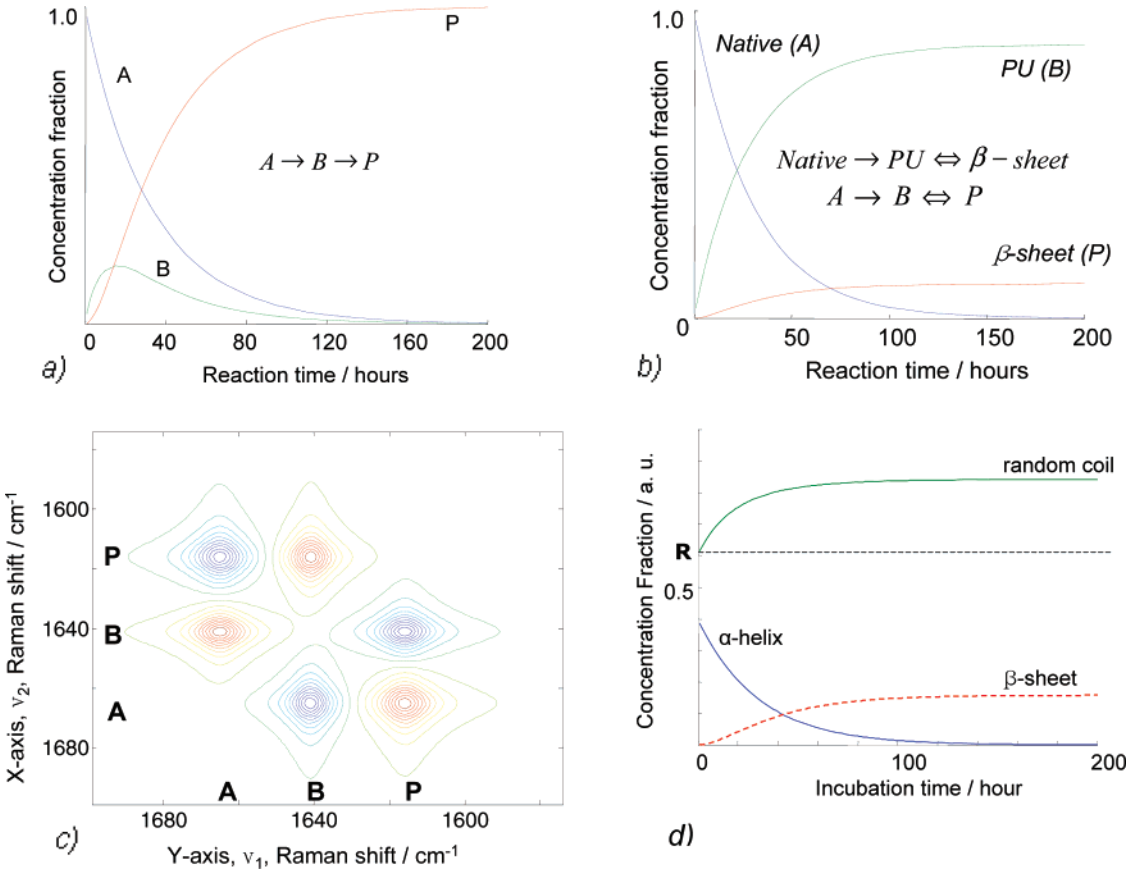

Figure 6. Sketch of concentration profiles of the reacting species for kinetic mechanism 1a (a), 1c or model 3 (b), and the asynchronous 2D map of the spectral data simulated for 1c kinetic mechanism (c). Simulated concentration profiles for model 2 (d). *R* level shows the fraction of disordered structure in native lysozyme.

We hypothesize that the transformations of lysozyme tertiary and secondary structures should follow the kinetics of some complex multistep chemical reaction. The concentration profiles modeling the behavior of the reacting species in several chemical reactions were simulated to produce model 2D maps. As a next step, the latter were compared with maps constructed from real DUVRR spectra of lysozyme.

The sequence of three spectroscopically distinguishable events—tertiary structure and α-helix melting → disordered structure formation → nucleus *β*-sheet formation—can be described by using one of the following reaction schemes:

$$\mathrm{A} \rightarrow \mathrm{B} \rightarrow \mathrm{P} \qquad (1a)$$

$$\mathrm{A} \leftrightarrow \mathrm{B} \rightarrow \mathrm{P} \qquad (1b)$$

$$\mathrm{A} \rightarrow \mathrm{B} \leftrightarrow \mathrm{P} \qquad (1c)$$

$$\mathrm{A} \leftrightarrow \mathrm{B} \leftrightarrow \mathrm{P} \qquad (1d)$$

In eqs 1a and 1b (see Figure 6a), the conversion of B to P is irreversible. As a consequence, the concentration of the intermediate B increases at the early stage of the reaction, resulting in negative correlation with A, and decreases during the rest of the reaction to yield positive correlation with A. Mechanisms 1c and 1d (Figure 6b), on the other hand, would result in negative correlation between the α-helix and disordered structure spectral contributions at all stages of the reaction. The latter was the case of our synchronous 2D-DUVRR maps (not shown), implying that the reaction mechanism involves equilibrium between disordered structure and newly formed *β*-sheet (1c or 1d). Further, the fact that the conversion of native lysozyme to the partially unfolded intermediate has been shown to be an irreversible transition[46] allowed us to finally postulate eq 1c as the actual reaction mechanism (model 2):

$$\alpha\text{-helix} \xrightarrow{k_1} \text{disordered structure} \underset{k_{-2}}{\overset{k_2}{\rightleftharpoons}} \beta\text{-sheet} \qquad (2)$$

As a next step, the rate constants of each process in reaction 2 were extracted based on the characteristic times found by the *kν* correlation analysis and previously reported[42] rate constants for the reaction (model 3):

$$\text{native} \xrightarrow{K_1} \text{PU} \underset{K_{-2}}{\overset{K_2}{\rightleftharpoons}} \text{nucleus} \qquad (3)$$

Noteworthy, the rate constants K_1, K_2, and K_{-2} in reaction 3 describe the evolution of native lysozyme, partially unfolded intermediate, and the *β*-sheet rich nucleus, while rate constants k_1, k_2, and k_{-2} refer to individual secondary structures. There is a major difference between the kinetics in models 2 and 3. Model 3 assumes (see Figure 6b) that all native lysozyme is converted to the partially unfolded intermediate, while effectively, only about 40% of native structure, α-helix and *β*-sheet, can melt as the remaining 60% of native lysozyme is initially in disordered structure.[45] Figure 6b,d depicts the difference between reaction schemes 2 and 3.

Specifically, Figure 6b shows the evolution profiles of native lysozyme, partially unfolded intermediate, and the *β*-sheet-rich nucleus constructed by using rate constants K_1, K_2, and K_{-2}

reported earlier.[42] Figure 6d sketches the evolution profiles of individual secondary structures provided that the fraction of disordered structure (R) in native lysozyme is equal to ~60%. The exact shapes of the evolution profiles (Figure 6d) depend on the unknown rate constants k_1, k_2, and k_{-2} in model 2 and therefore have to be evaluated. The simulation-aided $k\nu$ correlation approach proposed here allowed for calculating k_1, k_2, and k_{-2} constants and the evolution profiles for α-helix, disordered, and β-sheet structures.

The rigorous mathematical analysis of the integrated rate laws of reactions 2 and 3 (Supporting Information) yields the relation between rate constants K_1, K_2, and K_{-2} and k_1, k_2, and k_{-2} as follows:

$$k_1 = K_1$$
$$k_2 = K_2/(1 - R)$$
$$k_{-2} = K_{-2} - \frac{R}{1 - R} \times K_2 \quad (4)$$

where R is the fraction of disordered structure in native lysozyme.

To extract the rate constants k_1, k_2, and k_{-2} in model 2, the evolution profiles of secondary structures were simulated for different sets of rate constants k_i ($i = 1, 2, -2$). The spectral profiles of pure secondary structure spectra were modeled as mixed Gaussian−Lorentzian shapes. On the basis of the simulated evolution profiles and spectral shapes model DUVRR spectral sets were constructed followed by the calculation of corresponding $k\nu$ correlation maps. Comparison of simulated and experimental DUVRR $k\nu$ correlation maps enabled us to deduce the set of constants k_i ($i = 1, 2, -2$) based on the best match of correlation maps. When converted to the constants K_i ($i = 1, 2, -2$) for model 3 using eq 4, constants k_i ($i = 1, 2, -2$) turned out to be equal to the rate constants K_i ($i = 1, 2, -2$) previously reported by Shashilov et al.[42] The latter served as an additional proof of the validity of the proposed 2D correlation simulation-aided approach and the accuracy of the previously reported rate constants.

The characteristic times of individual reactions in models 2 and 3 taken as reciprocals of k_1, k_2, and k_{-2} equal $\tau_1 = 30$ h, $\tau_2 = 32$ h, $\tau_{-2} = 21$ h, provided that R equals 0.6[45] and $K_1 = 0.033$ h^{-1}, $K_2 = 0.0125$ h^{-1}, and $K_{-2} = 0.0067$ h^{-1}. Figure 5b shows the simulated asynchronous 2D map for the evolution of disordered structure and β-sheet structures with characteristic times $\tau_1 = 30$ h, $\tau_2 = 32$ h, $\tau_{-2} = 21$ h. For simplicity, the disordered structure and β-sheet C_α−H bending bands were simulated by the Gaussian shape centered at 1385 cm^{-1} and the Lorentzian one at 1400 cm^{-1}, respectively. As evident from Figure 5a,b, the pattern on the simulated 2D map matches one obtained from the experimental DUVRR spectra, producing the following apparent rates of secondary structure changes: disordered structure formation ($\tau \sim 22$ h) and nucleus β-sheet formation ($\tau \sim 35$ h). The latter verifies the validity of the proposed model 2 and the correctness of the estimated characteristic times τ_1, τ_2, and τ_{-2} of all reactions in model 2. Difference between measured and simulated DUVRR $k\nu$ correlation maps (Figure 5a,b) can be attributed to the contribution of adjacent Raman bands on the experimental $k\nu$ correlation map. Specifically, decrease in the characteristic time at 1380 cm^{-1} (Figure 5a) is probably due to the contribution of the C_α−$H_2(\beta)$ II band[44] of the β-sheet at ~1360 cm^{-1} that evolves with the same characteristic time as the C_α−H band located at ~1400 cm^{-1}.

It is worth noting that the $k\nu$ correlation analysis finds the best monoexponential fit to a kinetic profile in order to calculate the effective exponential characteristic time. The evolution profiles of the disordered and β-sheet structure in model 2 are the sum of two exponentials, whose decay times are expressed as linear combinations of characteristic times of elementary reactions in model 2 (Supporting Information). As a result, the monoexponential approximation of those biexponential profiles yields the effective characteristic times $\tau \sim 22$ and 36 h for the disordered and β-sheet structures, accordingly, which are not equal to any of the characteristic times ($\tau_2 = 32$ h, $\tau_{-2} = 21$ h) in the reaction scheme. On the other hand, helical and tertiary structures decay in a monoexponential fashion and thus have the effective $k\nu$ correlation characteristic times ($\tau \sim 30$ h) equal to the characteristic time of the elementary reaction α-helix → disordered in model 2. It should be emphasized that effective characteristic times are valuable because they enable one to find the true characteristic times of the elementary reactions. Namely, the true characteristic times of the reactions should result in the evolution profiles having the effective characteristic times extracted by using $k\nu$ correlation analysis.

Apparent Inverse Order of Events is the Intrinsic Property of Multistep Chemical Reactions. As seen from previous discussion, the reaction mechanism 1c and the corresponding model 2 produced the inverse order of events: disordered structure (B, intermediate) formation ($\tau \sim 22$ h) → tertiary structure and α-helix (initial reactant, A) melting ($\tau \sim 30$ h) → nucleus β-sheet (product, P) formation ($\tau \sim 35$ h). Our study showed that reactions 1a−1d all result in the apparent inverse order of events. Furthermore, it can be proven that any chemical reaction involving the formation of the intermediate(s) will lead to the inverse order of the events (Supporting Information).

We provide here a qualitative explanation to this effect, giving the strict mathematical justification in Supporting Information. The simulated concentration profiles for reaction 1c are sketched in Figure 6b. As seen from Figure 6b, the formation of the product exhibits a lag phase, which is typical for two- or multistep chemical reactions. Consider a simple two-state chemical reaction

$$A \rightarrow B \quad (5)$$

The integrated rate laws of reaction 5 are known to be simple exponential functions:

$$[A] = [A_0] \times \exp(-k_1 t) = [A_0] \times \exp(-t/\tau_1) \quad (6a)$$

$$[B] = [A_0] \times \{1 - \exp(-k_1 t)\} = [A_0] \times \{1 - \exp(-t/\tau_1)\} \quad (6b)$$

where k_1 and τ_1 are the rate constant and the characteristic time of the reaction, respectively.

As shown by Eads and Noda,[50] changes in spectral intensities expressed by exponential functions with equal decay rates do

(50) Eads, C. D.; Noda, I. *J. Am. Chem. Soc.* **2002**, *124*, 1111−1118.
(51) Tsuboi, M.; Suzuki, M.; Overman, S. A.; Thomas, G. J., Jr. *Biochemistry* **2000**, *39*, 2677−2684.
(52) Lednev, I. K.; Ermolenkov, V. V.; Higashiya, S.; Popova, L. A.; Topilina, N. I.; Welch, J. T. *Biophys. J.* **2006**, *91*, 3805−3818.
(53) Mikhonin, A. V.; Bykov, S. V.; Myshakina, N. S.; Asher, S. A. *J. Phys. Chem. B* **2006**, *110*, 1928−1943.

Table 2. Identifying the Type of the One- and Two-Step Reaction Based on 2D Correlation

observation		
intensities on synchronous map	intensities on asynchronous map[a]	possible mechanism
A and B negatively correlated	A and B are synchronous	A → B or A ↔ B
A and B negatively correlated at all stages of the reaction	B changes before A	A → B ↔ P or A ↔ B ↔ P
correlation of A and B changes sign over the course of the reaction[b]	sequential order A → P → B or B → A → P	A → B → P or A ↔ B → P

[a] Sequential order may change when varying the ratios of rate constants. Simulations using anticipated rate constants are advised when testing for all mechanisms. [b] This can also be the case for the reactions A ↔ B ↔ P and A → B ↔ P.

not give any contribution to asynchronous 2D maps. In another word, decay of A and formation of B in the case of reaction 5 would be synchronous. The reason for the inverse order in eq 1c is the formation of the product, P, which occurs with a lag phase. Since the total contribution of the intermediate B and product P evolves according to eq 6b, that is, in-phase with A, the intermediate B should change slightly ahead to compensate for the delay in product P formation. The magnitude of this effect mainly depends on the ratio of rate constants k_1, k_2, and k_{-2} in eq 1c. In general, the larger the ratio k_2/k_1 and k_2/k_{-2}, the larger the relative rate difference between the appearance of the intermediate and the decay of the reactant (see Supporting Information). Accordingly, the monoexponential approximation of the concentration profiles for A and B gives the larger effective rate or shorter characteristic time for the evolution of B, for example, $\tau \sim 30$ h for α-helix (A) and $\tau \sim 22$ h for disordered structure (B) in model 2.

The asynchronous 2D correlation map obtained from the spectral data modeling reaction mechanism 1c is depicted in Figure 6c. For simplicity, the spectral profiles of each reacting species were simulated as Lorentzian bands centered at 1665 cm^{-1} (A/α-helix), 1641 cm^{-1} (B/disordered structure), and 1616 cm^{-1} (P/β-sheet) and having bandwidths of 12, 10, and 12 cm^{-1}, respectively.[49] The corresponding 2D synchronous map (not shown) displays positive cross-peak at 1616/1641 cm^{-1} and negative ones at 1665/1641 and 1665/1616 cm^{-1}, which can be anticipated based on the given reaction scheme (Figure 6b). Analyzing the asynchronous 2D map (Figure 6c) reveals the following sequence of spectral changes 1641 cm^{-1} (B/disordered structure) → 1665 cm^{-1} →(A/α-helix) → 1616 cm^{-1} (P/β-sheet), which is consistent the 2D-DUVRR results of this study.

This study demonstrated that the *kυ* correlation analysis allows for quantitative assessment of the sequential order of events in terms of effective rate constants k_{eff} of each secondary structure evolution. This approach is superior to the representation of 2D results in terms of the sequential order of events as it allows for estimating the reaction-specific rate constants of secondary structure evolution.

Literature Reports on the Inverse Order of Events of Protein Folding Deduced from 2D Correlation Analysis. The apparent inverse order of the events observed in this study is worth taking into account as an alternative explanation of some previously reported results. In particular, the study of the formation of silk fibroin II by Zhou et al.[32] showed that the formation of silk fibroin, the product of the reaction, happened before the changes in the other secondary structures. The 2D-Raman/ROA analysis of the α-helix-to-β-sheet transition[39] clearly indicated that changes in the β-sheet, the product of the reaction, occurred before those in the α-helix. Although the abnormal sequential orders observed by Zhou et al.[32] and Ashton and co-workers[39] have been shown to have solid ground, one can hypothesize that the apparent inverse order effect may have implication in those 2D results. In particular, the α-helix-to-β-sheet transition of poly-L-lysine[39] may be the first step of fibril formation and, therefore, involve further transformation of a newly formed β-sheet into a fibrillar structure. If so, changes in the β-sheet structure would happen apparently before those in the α-helix, which might be the additional reason for the observed inverse order of structural rearrangements β-sheet→ α-helix.

Using the proposed approach for identifying the mechanism of the chemical reaction. The proposed simulation-aided approach can be easily generalized for any type of spectroscopic data and process under study. Table 2 summarizes the typical synchronous and asynchronous 2D intensity correlations for one- and two-step chemical reactions observed in our simulations. As seen from Table 2, the apparent order of events is mechanism-dependent and thus can be used for elucidating the reaction scheme of the (bio)chemical process. In any particular case, however, simulation of data using the kinetics with anticipated rate constants is advised for unambiguous interpretation of 2D correlation results.

Conclusion

In this study, we quantitatively characterized the kinetic mechanism of tertiary and secondary structural evolution of hen egg white lysozyme at the early stages of its fibrillation using the new 2D simulation-aided DUVRR approach. The proposed method circumvents the necessity of knowing the basis spectra of pure secondary structures, which are not observable experimentally and can be protein-specific. The proposed 2DCoS method is not limited to a particular spectroscopic technique and thus can be readily utilized for elucidating the mechanisms of complex (bio)chemical processes.

Acknowledgment. We are grateful to the reviewers of this manuscript for their positive evaluation of our work and numerous comments that improved the paper significantly.

Supporting Information Available: Matlab code for 2D correlation and *kυ* correlation analysis, derivation of eqs 4, and strict mathematical justification of the inverse sequential order effect. This material is available free of charge via the Internet at http://pubs.acs.org.

JA076225S